

# CARTS biogenesis requires VAP–lipid transfer protein complexes functioning at the endoplasmic reticulum–Golgi interface

Yuichi Wakana<sup>a</sup>, Richika Kotake<sup>a</sup>, Nanako Oyama<sup>a</sup>, Motohide Murate<sup>b</sup>, Toshihide Kobayashi<sup>b</sup>, Kohei Arasaki<sup>a</sup>, Hiroki Inoue<sup>a</sup>, and Mitsuo Tagaya<sup>a</sup>

<sup>a</sup>School of Life Sciences, Tokyo University of Pharmacy and Life Sciences, Hachioji, Tokyo 192-0392, Japan;

<sup>b</sup>Lipid Biology Laboratory, RIKEN, Wako, Saitama 351-0198, Japan

**ABSTRACT** Vesicle-associated membrane protein–associated protein (VAP) is an endoplasmic reticulum (ER)-resident integral membrane protein that controls a nonvesicular mode of ceramide and cholesterol transfer from the ER to the Golgi complex by interacting with ceramide transfer protein and oxysterol-binding protein (OSBP), respectively. We report that VAP and its interacting proteins are required for the processing and secretion of pancreatic adenocarcinoma up-regulated factor, whose transport from the *trans*-Golgi network (TGN) to the cell surface is mediated by transport carriers called “carriers of the *trans*-Golgi network to the cell surface” (CARTS). In VAP-depleted cells, diacylglycerol level at the TGN was decreased and CARTS formation was impaired. We found that VAP forms a complex with not only OSBP but also Sac1 phosphoinositide phosphatase at specialized ER subdomains that are closely apposed to the *trans*-Golgi/TGN, most likely reflecting membrane contact sites. Immobilization of ER–Golgi contacts dramatically reduced CARTS production, indicating that association–dissociation dynamics of the two membranes are important. On the basis of these findings, we propose that the ER–Golgi contacts play a pivotal role in lipid metabolism to control the biogenesis of transport carriers from the TGN.

## Monitoring Editor

Adam Linstedt  
Carnegie Mellon University

Received: Aug 26, 2015

Revised: Oct 7, 2015

Accepted: Oct 14, 2015

## INTRODUCTION

The Golgi complex is the central secretory organelle, performing glycoprotein maturation and the sorting of cargo molecules into

distinct transport carriers for secretion or delivery to various organelles. Previous work demonstrated that isolated Golgi membranes per se are capable of producing transport carriers in vitro (Balch *et al.*, 1984; Orci *et al.*, 1986; Malhotra *et al.*, 1989). In cells, however, the Golgi membranes contact the endoplasmic reticulum (ER) through specific sites called “membrane contact sites” (Ladinsky *et al.*, 1999; Mogelsvang *et al.*, 2004). Do these contact sites control functions of the Golgi complex?

Vesicle-associated membrane protein–associated protein (VAP) is an ER-resident type II membrane protein that can act as a molecular tether between the ER and other organelles through the interaction with lipids and/or lipid-binding proteins docked on the associated membranes (Loewen *et al.*, 2007; Rocha *et al.*, 2009; Manford *et al.*, 2012; Alpy *et al.*, 2013). In yeast, the VAP orthologues Scs2/Scs22 interact with oxysterol-binding homology protein 3 (Osh3) and Sac1 phosphoinositide phosphatase, and play a role in maintaining ER–plasma membrane (PM) contact sites and phosphoinositide signaling (Stefan *et al.*, 2011; 2013; Manford *et al.*, 2012). In mammalian cells, the interaction between VAP and oxysterol-binding protein (OSBP) has been suggested as controlling nonvesicular transport of cholesterol from the ER to the Golgi

This article was published online ahead of print in MBoC in Press (<http://www.molbiolcell.org/cgi/doi/10.1091/mbc.E15-08-0599>) on October 21, 2015.

Address correspondence to: Mitsuo Tagaya ([tagaya@toyaku.ac.jp](mailto:tagaya@toyaku.ac.jp)).

Abbreviations used: 25-OH, 25-hydroxycholesterol; Arf1, ADP-ribosylation factor 1; BSA, bovine serum albumin; CARTS, carriers of the *trans*-Golgi network to the cell surface; CERT, ceramide transfer protein; DAG, diacylglycerol; ER, endoplasmic reticulum; GFP, green fluorescent protein; GST, glutathione *S*-transferase; GT, galactosyltransferase; HA, hemagglutinin; mRFP, monomeric red fluorescent protein; OSBP, oxysterol-binding protein; Osh3, oxysterol-binding homology protein 3; PAUF, pancreatic adenocarcinoma up-regulated factor; PBS, phosphate-buffered saline; PC, phosphatidylcholine; PH, pleckstrin homology; PI, phosphatidylinositol; PI4K, phosphatidylinositol 4-kinase; PI4P, phosphatidylinositol 4-phosphate; PKD, protein kinase D; PLA, proximity ligation assay; PM, plasma membrane; SERCA2, sarco(endoplasmic reticulum Ca<sup>2+</sup> ATPase isoform 2; siRNA, small interfering RNA; SM, sphingomyelin; TGN, *trans*-Golgi network; VAP, vesicle-associated membrane protein–associated protein; VIMP, valosin-containing protein-interacting membrane protein; VSV-G, vesicular stomatitis virus G protein.

© 2015 Wakana *et al.* This article is distributed by The American Society for Cell Biology under license from the author(s). Two months after publication it is available to the public under an Attribution–Noncommercial–Share Alike 3.0 Unported Creative Commons License (<http://creativecommons.org/licenses/by-nc-sa/3.0>).

“ASCB®,” “The American Society for Cell Biology®,” and “Molecular Biology of the Cell®” are registered trademarks of The American Society for Cell Biology.

complex (Ngo and Ridgway, 2009; Mesmin *et al.*, 2013). An *in vitro* study revealed that VAP/OSBP-mediated sterol transfer is accompanied by reciprocal transfer of phosphatidylinositol 4-phosphate (PI4P), and these reactions are coupled to hydrolysis of PI4P by Sac1 (Mesmin *et al.*, 2013). VAP is also known to facilitate ceramide transport from the ER to the Golgi complex via the interaction with ceramide transfer protein (CERT), and thus regulates generation of sphingomyelin (SM) and diacylglycerol (DAG) from ceramide and phosphatidylcholine (PC) at the *trans*-Golgi membranes (Hanada *et al.*, 2003; 2009; Perry and Ridgway, 2005; 2006; Kawano *et al.*, 2006; Peretti *et al.*, 2008). Electron microscope tomography revealed that subregions of the ER and the *trans*-Golgi membranes form close contacts, and they have been proposed to function as sites for VAP-mediated nonvesicular lipid transfer (Ladinsky *et al.*, 1999; Mogelvang *et al.*, 2004; Hanada *et al.*, 2009; Mesmin *et al.*, 2013).

In this study, we investigated a role for VAP in the biogenesis of a new class of *trans*-Golgi network (TGN)-derived transport carriers called CARTS (carriers of the TGN to the cell surface). We previously reported that CARTS transport cargoes, such as pancreatic adenocarcinoma up-regulated factor (PAUF), TGN46, and lysozyme C, from the TGN to the cell surface in a microtubule- and kinesin-5-dependent manner, and their biogenesis requires protein kinase D (PKD)-mediated membrane fission (Wakana *et al.*, 2012; 2013). In this paper, we describe the molecular mechanism by which VAP regulates CARTS formation upstream of PKD. Our study provides evidence that the ER–Golgi contacts play an important role in regulating transport carrier biogenesis from the TGN.

## RESULTS

### VAPs are required for the processing and secretion of PAUF

Lev and colleagues (Peretti *et al.*, 2008) reported that depletion of VAP inhibited transport of vesicular stomatitis virus G protein (VSV-G) from the TGN to the cell surface. We have previously shown that the TGN to cell surface carriers CARTS exclude VSV-G and are therefore distinct from VSV-G-containing carriers (Wakana *et al.*, 2012). To test the requirement of VAP for CARTS-mediated transport, we first examined the effects of VAP knockdown on secretion of one of their cargo proteins, PAUF. There are two isoforms of VAP, VAP-A and VAP-B, which share a high sequence homology and can form homo- and heterodimers (Nishimura *et al.*, 1999; Lev *et al.*, 2008). For reducing the expression of both VAP isoforms, HeLa cells were transfected with a mixture of small interfering RNA (siRNA) oligos specific for VAP-A and VAP-B. At 72 h after siRNA transfection, the expression levels of VAP-A and VAP-B were reduced by ~80% compared with control cells (Figure 1A). For monitoring the secretion of PAUF, control and VAP-A/B knockdown cells were transfected with a plasmid for MycHis-tagged PAUF; 20 h later, the cells were washed and incubated with fresh medium. At the indicated time points, a portion of the medium was collected and Western blotted with an anti-His antibody. The data reveal that VAP-A/B knockdown reduced PAUF-MycHis secretion by more than 50% compared with control cells (Figure 1B), suggesting that VAPs are required for the CARTS-mediated transport. The intracellular pool of PAUF is modified and secreted as a higher-molecular-weight mature-form protein (Kim *et al.*, 2009; Wakana *et al.*, 2012). In VAP-A/B knockdown cells, however, an immature form of PAUF-MycHis was secreted (Figure 1B, asterisk). This result suggests that VAP-A/B knockdown impaired the processing of PAUF and its secretion. To exclude the possibility of off-target effects of the siRNA oligos, we tested another set of siRNA oligos, and similar results were obtained (Supplemental Figure S1, A and B).

### VAPs regulate PAUF processing and secretion via lipid transfer between the ER and the Golgi complex

Ceramide transported by VAP/CERT is converted, together with PC, to SM and DAG by SM synthase at the *trans*-Golgi membranes (Huitema *et al.*, 2004; Hanada *et al.*, 2009). Previous work reported that depletion of VAPs reduced both SM and DAG levels (Perry and Ridgway, 2006; Peretti *et al.*, 2008). To confirm that the lipid homeostasis at the TGN was affected in our knockdown procedure, we examined DAG-dependent recruitment of the membrane fission factor PKD to the TGN. Control and VAP-A/B knockdown cells were transfected with a plasmid for glutathione S-transferase (GST)-tagged C1a domain of PKD1 (GST-C1a-PKD1) that binds to DAG (Maeda *et al.*, 2001; Baron and Malhotra, 2002) or a plasmid for GST-tagged full-length PKD2. In VAP-A/B knockdown cells, the fluorescence signals of TGN-localized GST-C1a-PKD1 and GST-PKD2 were reduced compared with control cells (Figure 1C), which is consistent with a previous report (Peretti *et al.*, 2008).

Next we examined whether 25-hydroxycholesterol (25-OH), which binds to OSBP with high affinity and inhibits VAP/OSBP-mediated sterol transfer (Mesmin *et al.*, 2013), influences the effects of VAP-A/B knockdown on PAUF processing and secretion. This reagent is also known to inhibit cholesterol synthesis (Brown and Goldstein, 1974; Kandutsch and Chen, 1974). In control cells, there was no significant effect of 25-OH, whereas in VAP-A/B knockdown cells, the inhibitory effects on both the processing and secretion of PAUF-MycHis became more pronounced upon 25-OH treatment (Figure 1D).

Cholesterol and sphingolipids assemble into lipid microdomains segregated from other lipids in the membranes, and these lipid microdomains have been reported to function together with specific proteins as a platform for regulating membrane signaling and trafficking (Simons and Ikonen, 1997; Lingwood and Simons, 2010; Simons and Sampaio, 2011). We hypothesized that inhibition of VAP-mediated lipid transfer results in disruption of cholesterol- and SM-rich microdomain organization at the TGN membranes and thereby impairs the processing and export of PAUF from the TGN. Because the function of SM-rich microdomains can be disrupted by *D*-ceramide-C6 that is converted to a short-chain C6-SM (Duran *et al.*, 2012; van Galen *et al.*, 2014), HeLa cells expressing PAUF-MycHis were treated with the reagent. The results show that *D*-ceramide-C6 treatment inhibited PAUF-MycHis processing and secretion, similar to VAP-A/B knockdown (Figure 1E).

Next we asked whether double knockdown of CERT and OSBP causes the same effects as VAP-A/B knockdown. Reverse transcription PCR (RT-PCR) revealed that the knockdown by a mixture of siRNA oligos targeting CERT and OSBP (C+O siRNA) led to a reduction of greater than 80% in the mRNA levels of these proteins (Figure 2A). The amount of PAUF-MycHis secreted from CERT/OSBP double-knockdown cells was decreased by 32% compared with control cells, accompanied by an increase in the ratio of the immature to mature form of PAUF-MycHis (Figure 2B). Similar to VAP-A/B knockdown, these effects were augmented in the presence of 25-OH (Figure 2C). In cells depleted of OSBP alone, the expression levels of PAUF-MycHis were reduced and the amount of secreted proteins normalized with the total cellular levels showed a 19% reduction compared with control cells (Supplemental Figure S1C). We also tested the effects of dominant-negative FF/AA mutants of CERT and OSBP, which harbor replacement of two phenylalanines in their FFAT (two phenylalanines in acidic tract) motif with alanines, and thus cannot interact with VAPs (Wyles *et al.*, 2002; Loewen *et al.*, 2003; Kawano *et al.*, 2006; Perry and Ridgway, 2006). For this purpose, HEK 293T cells were transfected with a PAUF-MycHis plasmid alone

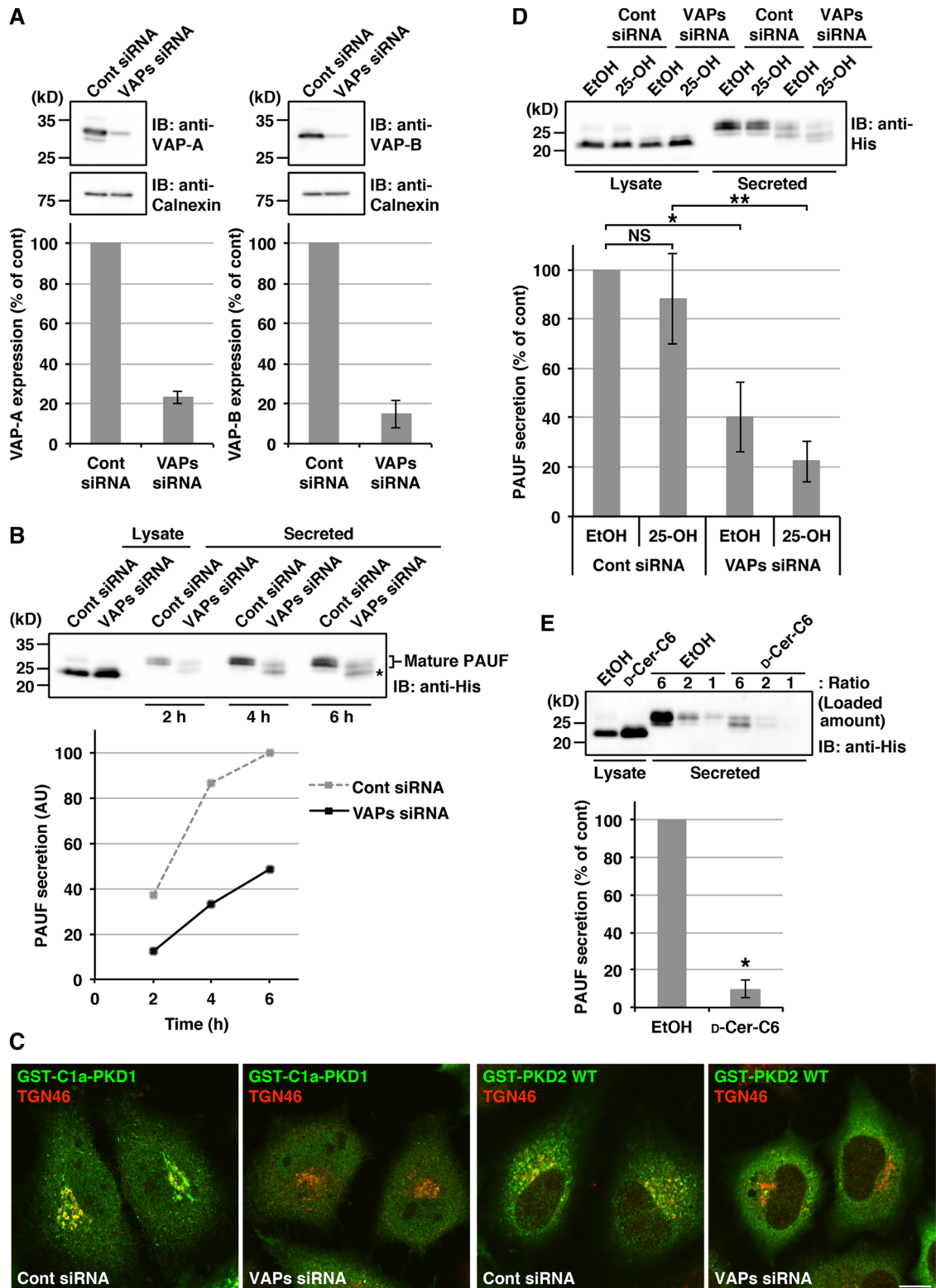


**FIGURE 1:** VAP-A/B knockdown inhibits the processing and secretion of PAUF. (A–D) HeLa cells were transfected with control (Cont) siRNA or a mixture of siRNA oligos specific for VAP-A (523) and VAP-B (498). (A) At 72 h after siRNA transfection, the cell lysates were collected and Western blotted with the indicated antibodies. Calnexin was used as a marker to monitor the amount of proteins loaded. The graphs show quantification of the expression levels of VAPs. The average values of four independent experiments are shown (mean  $\pm$  SD). (B and D) At 48 h after siRNA transfection, the cells were transfected with a plasmid for PAUF-MycHis. (B) After 20 h, the cells were washed and incubated with fresh medium, and a portion of medium was collected at the indicated time points. (D) The cells were pretreated with ethanol (EtOH) or 2  $\mu$ g/ml 25-OH for 2.5 h and further incubated with fresh medium containing each reagent for 3 h. The medium and the cell lysate were Western blotted with an anti-His antibody. Asterisk in B denotes the immature form of

(control) or with a PAUF-MycHis plasmid in combination with a plasmid for the wild type or the FF/AA mutant of hemagglutinin (HA)-tagged CERT or Myc-tagged OSBP. Both CERT and OSBP FF/AA mutants substantially impaired the processing and secretion of PAUF (Figure 2, D and E), indicating that VAPs regulate PAUF processing and secretion through interaction with CERT and OSBP.

### VAPs are required for membrane fission during CARTS biogenesis

Our data so far obtained raise the possibility that VAPs regulate PAUF processing and secretion through at least two different events: 1) DAG production followed by PKD recruitment to the TGN, and 2) cholesterol- and SM-rich microdomain organization at the TGN. To investigate the roles of VAP-mediated lipid signaling in the biogenesis of CARTS, we visualized PAUF-MycHis-containing CARTS in HeLa cells by fluorescence microscopy. As shown previously (Wakana *et al.*, 2012), PAUF-MycHis in control cells was localized to the pericentriolar Golgi region with a number of peripheral small punctate elements corresponding to CARTS (Figure 3A, top, left panel). On the other hand, in VAP-A/B knockdown cells, tubular structures were observed to be extended from the Golgi membranes (Figure 3A, top, right panel). The number of cells containing such tubules was significantly increased upon 25-OH treatment following VAP-A/B knockdown, whereas there was almost no change in control cells after the treatment (Figure 3, A, bottom panels, and B). It has been previously shown that the overexpression of a dominant-negative kinase-dead mutant of PKD causes the formation of cargo-containing tubules as a result of impaired scission of the TGN membranes (Liljedahl *et al.*, 2001; Wakana *et al.*, 2012). Consistent with this, in cells in which PAUF-MycHis-containing large tubules were formed, the average number of CARTS was decreased to one-third of control cells (Figure 3C). PAUF-MycHis-containing tubules also formed in CERT/OSBP double-knockdown cells but were not detected in either CERT or OSBP single-knockdown cells (Supplemental Figure S2).

### VAPs are required for the biogenesis of CARTS in permeabilized cells

We further investigated the effects of VAP-A/B knockdown on CARTS biogenesis by using a biochemical assay that we established previously (Wakana *et al.*, 2012). Control and VAP-A/B knockdown cells were treated with 25-OH and permeabilized with digitonin. The permeabilized cells were then incubated in the presence of an ATP-regenerating system and rat liver cytosol at 32°C or, as a negative control, at 4°C. CARTS-containing fractions were collected by high-speed centrifugation and Western blotted with an antibody against TGN46, a cargo protein in CARTS (Wakana *et al.*, 2012). TGN46 is a heavily glycosylated protein, and major polypeptides are detected as a band of ~110 kDa in HeLa cell lysates (Prescott *et al.*, 1997). On VAP-A/B knockdown, TGN46 was detected as a more smeared band compared with the control (Figure 3D), which is reminiscent of the observed defects in the processing

of PAUF-MycHis (Figure 1, B and D). The amount of CARTS produced at 32°C was normalized with the starting materials (permeabilized cells: input) and quantified. The results indicate a 30% reduction upon VAP-A/B knockdown compared with the control (Figure 3, D and E).

### VAPs and Sac1 accumulate at juxtannuclear ER subdomains closely apposed to the *trans*-Golgi/TGN

In HeLa cells, both VAP-A and VAP-B exhibit a reticular distribution that is a common feature of ER-localized proteins (Supplemental Figure S3A). The immunostaining specificity of our antibodies against VAP-A and VAP-B is validated by the fact that knockdown of the respective VAP isoforms reduced their staining (Supplemental Figure S3B). It was recently reported that ER-localized Sac1 phosphoinositide phosphatase regulates VAP/OSBP-mediated cholesterol transfer from the ER to the *trans*-Golgi (Mesmin *et al.*, 2013). We therefore examined whether VAP and Sac1 potentially accumulate at specialized ER subdomains that are closely apposed to the *trans*-Golgi/TGN and responsible for nonvesicular lipid transfer between these two compartments. Because there are no anti-Sac1 antibodies available for immunofluorescence, HeLa cells stably expressing green fluorescent protein (GFP)-fused Sac1 were used. GFP-Sac1 showed a reticular distribution, as well as juxtannuclear structures that resemble the Golgi complex, as previously reported (Rohde *et al.*, 2003; Liu *et al.*, 2008; Wang *et al.*, 2013). It should be noted that Sac1 was reported to traffic to the Golgi complex in quiescent cells (Blagoveshchenskaya *et al.*, 2008). Of interest, we detected endogenous VAPs in the perinuclear small punctate elements, where they colocalized with GFP-Sac1 (Supplemental Figure S3C). Strikingly, 25-OH treatment significantly increased an accumulation of VAPs, especially VAP-A, in the GFP-Sac1-positive juxtannuclear structures (Figure 4, A, third and fourth rows, and B, right graph). An ER marker, sarco(endo)plasmic reticulum Ca<sup>2+</sup> ATPase isoform 2 (SERCA2) did not show such accumulations (Figure 4A, bottom row), suggesting the specificity of VAPs for targeting to these juxtannuclear compartments. The fluorescence of GFP-Sac1 showed limited overlap with that of TGN46 (Figure 4, A, top and second rows, and B, left graph), suggesting the possibility that the GFP-Sac1- and VAPs-positive juxtannuclear compartments are associated with the ER membrane, rather than the Golgi membranes.

To validate this possibility, we performed two experiments. First, we treated GFP-Sac1-expressing cells with the microtubule depolymerizing reagent nocodazole. Nocodazole is known to disperse the Golgi membranes into a number of smaller elements retaining their *cis-trans* polarity (Cole *et al.*, 1996; Shima *et al.*, 1997). In nocodazole-treated cells, colocalization of GFP-Sac1 with VAPs was prominent in a number of small punctate elements, compared with the colocalization with TGN46 (Supplemental Figure S4). We next performed fluorescence loss in photobleaching experiments (Figure 5). Photobleaching of the peripheral area marked by a red line clearly decreased a fluorescence signal of GFP-Sac1 in the peripheral region and caused a subsequent decrease in the

---

PAUF. The graphs show quantification of PAUF secretion. The amount of secreted PAUF was normalized with the total cellular levels. The average values of three independent experiments are shown in the graph in D (mean ± SD). Single and double asterisks in D indicate  $p < 0.05$  and  $p < 0.01$ , respectively. (C) At 48 h after siRNA transfection, the cells were transfected with a plasmid for GST-C1a-PKD1 or GST-PKD2 wild type (WT). After 20 h, the cells were fixed and visualized with anti-GST and anti-TGN46 antibodies. Scale bar: 10 μm. (E) HeLa cells were transfected with a plasmid for PAUF-MycHis. After 20 h, the cells were pretreated with ethanol (control) or 5 μM D-ceramide-C6 (D-Cer-C6) for 2.5 h and further incubated with fresh medium containing each reagent for 3 h. Western blotting and quantification were performed as in D. Asterisk indicates  $p < 0.0005$ .

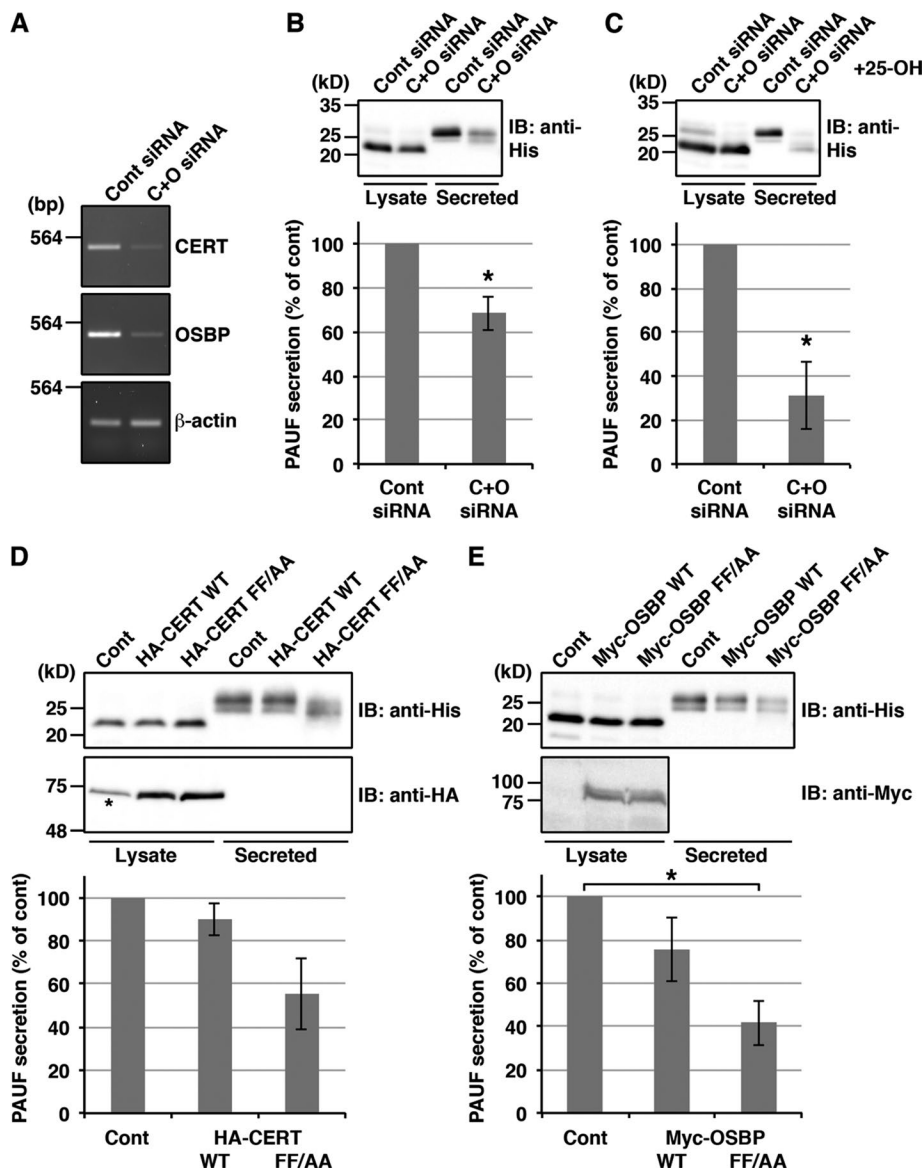


**FIGURE 2:** Disruption of the functions of CERT and OSBP inhibits the processing and secretion of PAUF. (A–C) HeLa cells were transfected with control (Cont) siRNA or a mixture of siRNA oligos specific for CERT and OSBP (C+O siRNA). (A) At 72 h after siRNA transfection, RNA was prepared from the cells, and the knockdown efficiency was monitored by RT-PCR with specific primers for CERT, OSBP, or  $\beta$ -actin. (B and C) At 48 h after siRNA transfection, the cells were transfected with a plasmid for PAUF-MycHis. (B) After 20 h, the cells were washed and incubated with fresh medium for 6 h. (C) The cells were pretreated with 2  $\mu$ g/ml 25-OH for 2.5 h and further incubated with fresh medium containing 25-OH for 3 h. Western blotting and quantification were performed as in Figure 1D. The average values of three and five independent experiments are shown in the graphs in B and C, respectively (mean  $\pm$  SD). Asterisks indicate  $p < 0.02$  (B) and  $p < 0.005$  (C). (D and E) HEK 293T cells were transfected with a PAUF-MycHis plasmid alone (Cont) or with a PAUF-MycHis plasmid in combination with a plasmid for the wild type (WT) or the FF/AA mutant of HA-CERT (D) or Myc-OSBP (E). After 20 h, the cells were washed and incubated with fresh medium for 4 h. The medium and the cell lysate were Western blotted with the indicated antibodies. Quantification was performed as in Figure 1D. Asterisk in D denotes a nonspecific polypeptide, and asterisk in E indicates  $p < 0.02$ .

perinuclear signal accompanied by dispersion of the fluorescence to the periphery (Figure 5, A, top row, and B, blue line). In contrast, there was no significant decrease in the fluorescence signal of Golgi-localized GFP-galactosyltransferase (GT; Figure 5, A, bottom row, and B, red line). These results indicate the continuity of the GFP-Sac1-positive juxtannuclear compartments with the peripheral

VAPs and OSBP takes place at the Sac1-positive juxtannuclear compartments, we performed a proximity ligation assay (PLA). In this assay a fluorescence signal is observed if two proteins are in close proximity (within 30–40 nm; Söderberg *et al.*, 2006). We found that the PLA signals for VAP-A and Myc-OSBP were partially overlapped with the fluorescence of GFP-Sac1 in the juxtannuclear

ER and suggest that Sac1 and VAPs accumulate at juxtannuclear ER subdomains closely apposed to the *trans*-Golgi/TGN.

### Sac1 forms a complex with VAPs and OSBP at juxtannuclear ER subdomains

To gain further insight into the mechanism underlying accumulation of Sac1 and VAPs at juxtannuclear ER subdomains, we tested the interaction of these proteins. FLAG-tagged Sac1 was expressed in HEK 293T cells and immunoprecipitated with anti-FLAG beads. As shown in Figure 6A, endogenous VAP-A and VAP-B were coprecipitated with FLAG-Sac1 (lane 7). FLAG-Sac1 showed a higher affinity for VAP-A than VAP-B, which is consistent with more marked colocalization of Sac1 with VAP-A than VAP-B at the juxtannuclear compartments (Figure 4A), although 25-OH treatment did not significantly affect their interactions (Figure 6A, lane 8). Other ER integral membrane proteins, calnexin and valosin-containing protein-interacting membrane protein (VIMP), were not coprecipitated with FLAG-Sac1 (Figure 6A, lanes 7 and 8), suggesting that the interaction of VAPs with FLAG-Sac1 is specific. Next we examined whether overexpression of OSBP or CERT affects the interaction. FLAG-Sac1 and Myc-OSBP or HA-CERT were coexpressed and immunoprecipitated with anti-FLAG beads. Myc-OSBP but not HA-CERT was coprecipitated with FLAG-Sac1, and the amount of coprecipitated VAPs was increased only by overexpression of Myc-OSBP (Figure 6, B, lane 4, and C, lane 4). When a VAP-binding deficient mutant of OSBP (FF/AA) was coexpressed with FLAG-Sac1, no increase in VAP coprecipitation was observed (Figure 6B, lane 8). These results suggest that Sac1 forms a complex with VAPs and OSBP but not CERT.

Next localization of OSBP was compared with that of Sac1 and VAPs in HeLa cells. We found that coexpression of Myc-OSBP and GFP-Sac1 caused an accumulation of VAPs, and all these proteins showed colocalization at the juxtannuclear compartments (Figure 6D). Although HA-CERT was present throughout the cytoplasm (Supplemental Figure S5, top row), this protein was also detected at the GFP-Sac1-positive juxtannuclear compartments after treatment of cells with digitonin to remove cytosolic proteins (Supplemental Figure S5, bottom row). To ascertain that the interaction of

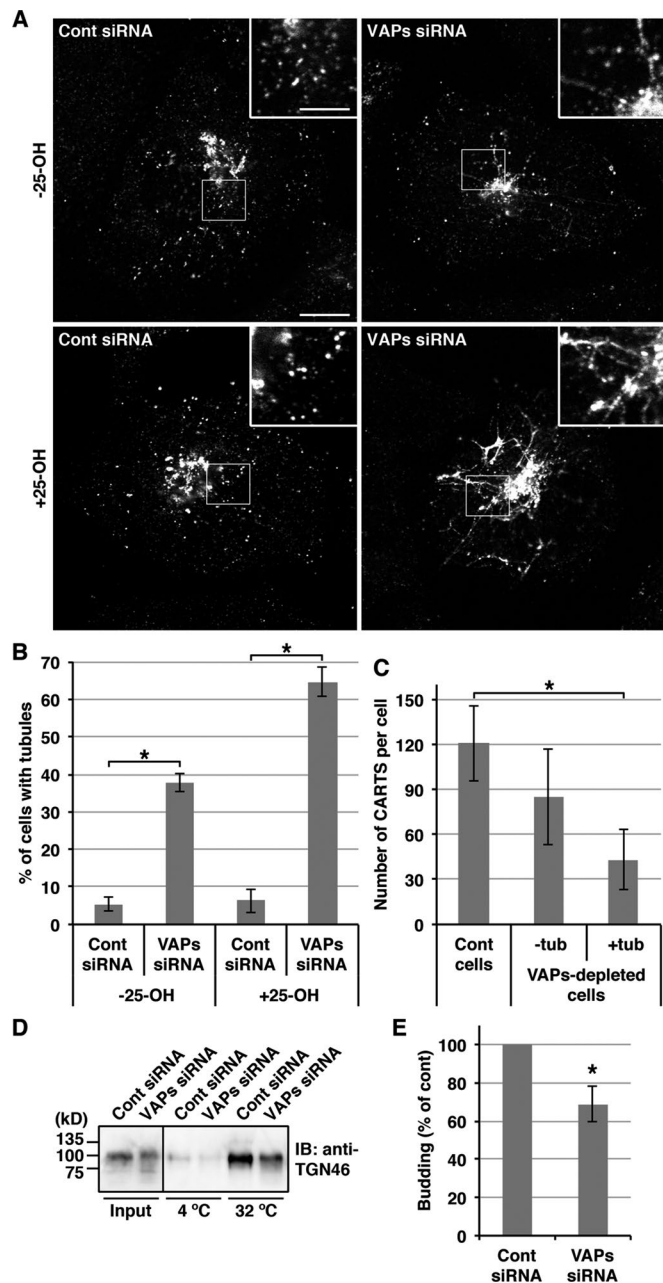


**FIGURE 3:** VAP-A/B knockdown inhibits the biogenesis of CARTS from the TGN. (A–C) HeLa cells stably expressing PAUF-MycHis were transfected with control (Cont) siRNA or a mixture of siRNA oligos specific for VAP-A (523) and VAP-B (498). After 72 h, the cells were treated with or without 2  $\mu\text{g/ml}$  25-OH for 2.5 h, fixed, and visualized with an anti-Myc antibody. High magnifications of the boxed areas are shown in the insets. Scale bars: 10  $\mu\text{m}$  (large panels); 4  $\mu\text{m}$  (insets). (B) Quantification of the formation of PAUF-MycHis-containing tubules. The percentage of control and VAP-A/B knockdown cells with PAUF-MycHis-containing tubules in the presence or absence of 25-OH ( $n = 102$ –123 cells per condition) was determined, and the average values of four independent experiments are shown (mean  $\pm$  SD). Asterisks indicate  $p < 0.0001$ . (C) Quantification of PAUF-MycHis-containing CARTS. The number of CARTS in 25-OH-treated control cells ( $n = 1208$  punctate elements in 10 cells) and VAP-A/B-depleted cells with or without large tubules (tub) ( $n = 432$  and 850 punctate elements in 10 cells, respectively) was determined (mean  $\pm$  SD). Asterisk indicates  $p < 0.0001$ . (D and E) HeLa cells were transfected with control siRNA or a mixture of siRNA oligos specific for VAP-A (523) and VAP-B (498). At 72 h after siRNA transfection, the cells were treated with

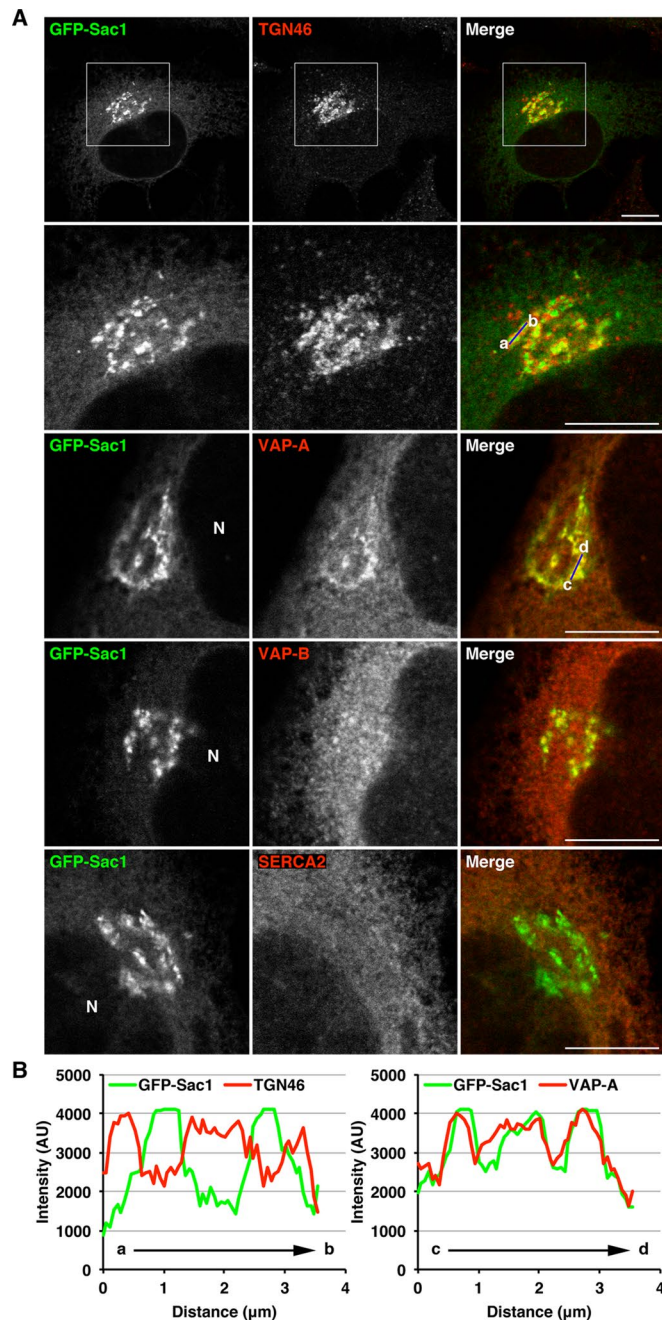


**FIGURE 4:** Colocalization of VAPs with Sac1 at juxtannuclear compartments closely apposed to the TGN. (A and B) HeLa cells stably expressing GFP-Sac1 were treated with 2  $\mu\text{g/ml}$  25-OH for 1 h, fixed, and visualized with GFP and an antibody against TGN46, VAP-A, VAP-B, or SERCA2. High magnifications of the boxed areas are shown in the lower panels. N, nucleus. Scale bars: 10  $\mu\text{m}$ . (B) Distribution of GFP-Sac1 and TGN46 (left graph) or VAP-A (right graph) in the perinuclear region. The fluorescence intensity of GFP-Sac1 and TGN46 or VAP-A along a blue line in the respective merged images is shown.

2  $\mu\text{g/ml}$  25-OH for 2.5 h and subjected to CARTS formation assay as described in *Materials and Methods*. The pellet produced with high-speed centrifugation and containing CARTS was Western blotted with an anti-TGN46 antibody. The input refers to permeabilized HeLa cells used as starting material in these experiments. (E) Quantification of CARTS formation. The average values of four experiments are shown (mean  $\pm$  SD). Asterisk indicates  $p < 0.03$ .

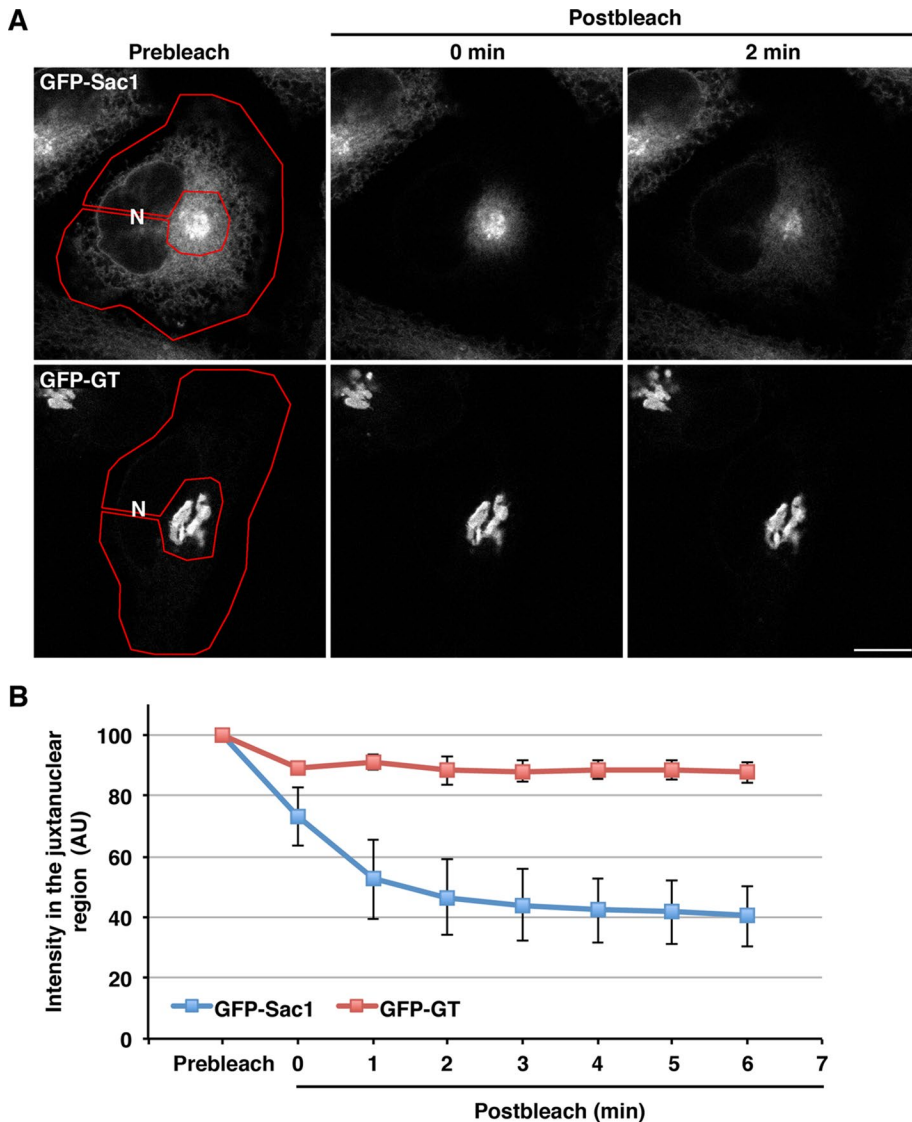


**FIGURE 5:** Sac1-positive juxtannuclear compartments are associated with the ER membrane. (A) HeLa cells stably expressing GFP-Sac1 or GFP-GT were subjected to fluorescence loss in photobleaching. The areas marked by a red line were bleached as described in *Materials and Methods*. Scale bar: 10  $\mu$ m. (B) Quantification of the fluorescence intensity of GFP-Sac1 and GFP-GT in the juxtannuclear region. The average values of the fluorescence intensity of three cells at the indicated time points are shown (mean  $\pm$  SD).

region (Figure 6E, top row). On overexpression of a phosphatase-dead Sac1 mutant (Cys-389 is replaced with serine: C/S; Rohde *et al.*, 2003), more PLA signals were detected and they showed strong overlap with the fluorescence of the GFP-Sac1 mutant in the juxtannuclear region (Figure 6E, bottom row).

If Sac1 accumulates in the juxtannuclear region as a consequence of its interactions with VAPs and OSBP, one may expect that knockdown of VAPs and/or OSBP affects Sac1 distribution. Figure 7 shows this to be the case: VAP-A/B knockdown significantly inhibited juxtannuclear accumulations of GFP-Sac1 upon 25-OH treatment, although the effects were weak in the absence of the reagent (Figure 7, A, middle row, and B). Knockdown of OSBP but not CERT strongly inhibited the accumulations of GFP-Sac1, even in the absence of 25-OH (Figure 7, A, bottom row, and B), suggesting a direct role of OSBP in regulating the juxtannuclear localization of Sac1. Consistent with this finding, recruitment of OSBP was impaired in VAP-A/B

knockdown cells, especially upon 25-OH treatment (Figure 7C), as previously reported (Peretti *et al.*, 2008).

Altogether these results suggest the presence of VAP-OSBP-Sac1 and VAP-CERT complexes at the specialized ER subdomains closely apposed to the *trans*-Golgi/TGN, which are thought to form ER-Golgi contacts.

### Sac1 regulates the processing and secretion of PAUF in a phosphatase activity-dependent manner

To demonstrate the functional link among Sac1, VAPs, and OSBP, we asked whether Sac1 regulates the processing and secretion of PAUF. HEK 293T cells were cotransfected with plasmids encoding PAUF-MycHis and GFP (control), GFP-Sac1 wild type, or the phosphatase-dead mutant (C/S). Overexpression of GFP-Sac1 wild type reduced PAUF-MycHis secretion by 89% compared with control cells (Figure 8A). We found that immature forms of PAUF-MycHis were secreted in these cells, as seen in VAP-A/B knockdown cells and the cells in which the functions of CERT and OSBP were perturbed (Figures 1, B and D, and 2, B–E). The phosphatase-dead mutant showed less effect than the wild type, suggesting that Sac1 regulates PAUF processing and secretion via hydrolysis of PI4P, which is consistent with the finding that hydrolysis of PI4P by Sac1 is required for VAP/OSBP-mediated sterol transfer in vitro (Mesmin *et al.*, 2013). Previous work reported that overexpression of the wild type or the constitutively Golgi-localized mutant of Sac1 (K2A) depletes Golgi PI4P levels (Blagoveshchenskaya *et al.*, 2008; Dippold *et al.*, 2009; Hammond *et al.*, 2014). To monitor PI4P levels, we used the PI4P sensor FAPP-PH-GST (GST-tagged pleckstrin homology [PH] domain of four-phosphate adaptor protein; Dowler *et al.*, 2000). In cells in which GFP-Sac1 wild type was highly

expressed, juxtannuclear signals of FAPP-PH-GST disappeared, whereas a compact juxtannuclear distribution of FAPP-PH-GST was observed in cells with high expression of the phosphatase-dead mutant (Figure 8B). Consistent with a previous finding that OSBP binds PI4P via its PH domain for targeting to the Golgi membrane (Levine and Munro, 2002), high-level expression of GFP-Sac1 wild type impaired recruitment of Myc-OSBP (Figure 8C).

### Association-dissociation dynamics of ER-Golgi contacts are important for CARTS biogenesis

Antony and colleagues (Mesmin *et al.*, 2013) demonstrated by electron microscopy that an OSBP construct, PH-FFAT, which contains the PH domain, coiled-coil region, and FFAT motif, fixed and expanded ER-Golgi contacts. Taking advantage of this construct, we sought to demonstrate the implication of ER-Golgi contacts in CARTS biogenesis. When Myc-PH-FFAT was expressed in HeLa

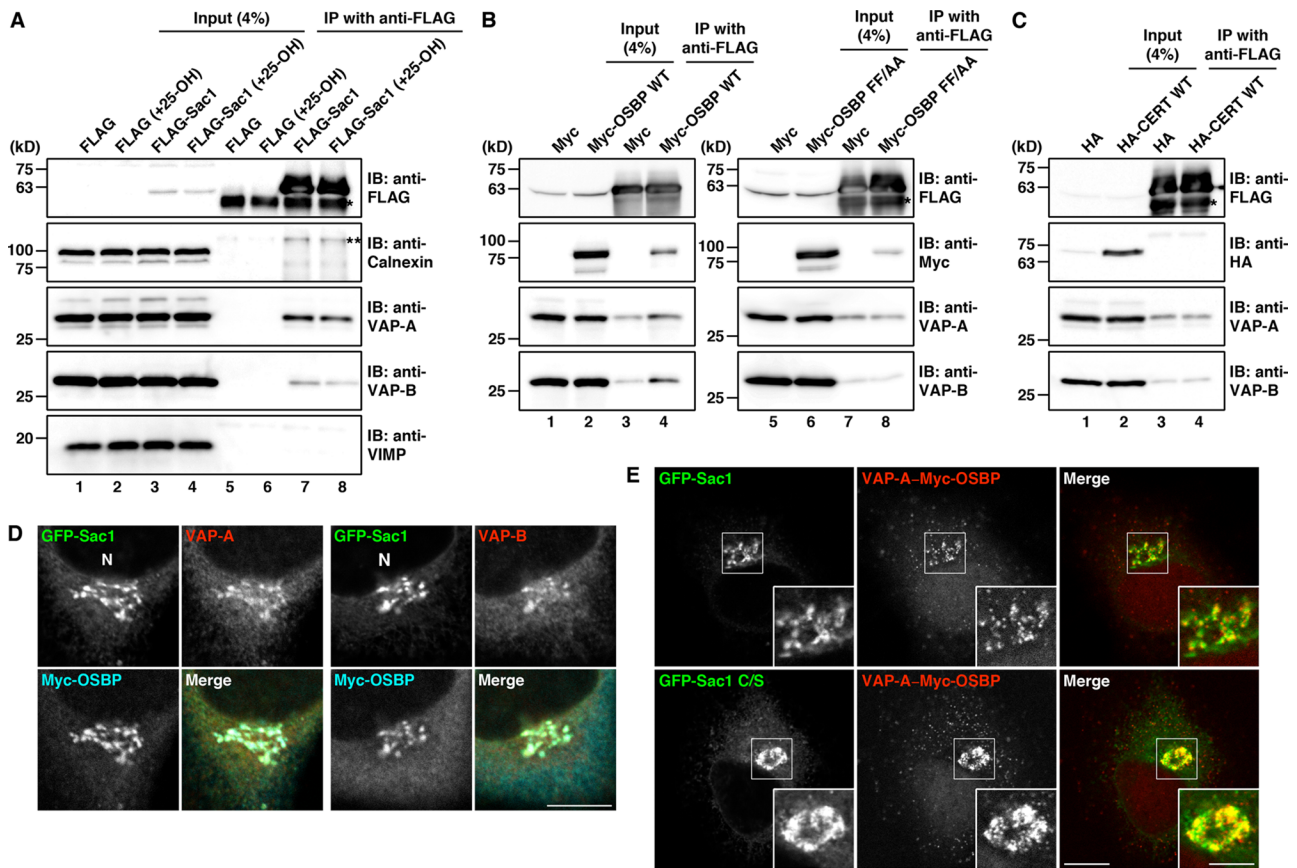


**FIGURE 6:** Interaction and colocalization of Sac1 with VAPs and OSBP at juxtannuclear ER subdomains. (A) HEK 293T cells were transfected with a plasmid for FLAG-Sac1 or the FLAG vector; 20 h later, the cells were treated with ethanol or 4  $\mu\text{g/ml}$  25-OH for 2.5 h. The cell lysates were subjected to immunoprecipitation with anti-FLAG beads. The cell lysates (input) and immunoprecipitates were Western blotted with the indicated antibodies. The single and double asterisks denote immunoglobulin heavy chain and a nonspecific polypeptide, respectively. (B) Lysates of HEK 293T cells transfected with plasmids for FLAG-Sac1 and Myc-OSBP wild type (WT) or FF/AA or the Myc vector were subjected to immunoprecipitation with anti-FLAG beads. Asterisk denotes immunoglobulin heavy chain. (C) Lysates of HEK 293T cells transfected with plasmids for FLAG-Sac1 and HA-CERT or the HA vector were subjected to immunoprecipitation with anti-FLAG beads. Asterisk denotes immunoglobulin heavy chain. (D) HeLa cells were cotransfected with plasmids for GFP-Sac1 and Myc-OSBP, fixed, and visualized with GFP and antibodies against Myc and VAP-A or VAP-B. N, nucleus. Scale bar: 10  $\mu\text{m}$ . (E) HeLa cells stably expressing GFP-Sac1 were transfected with a plasmid for Myc-OSBP (top row). For the experiment with GFP-Sac1 C/S (bottom row), HeLa cells were cotransfected with plasmids for GFP-Sac1 C/S and Myc-OSBP. The cells were fixed and subjected to PLA with antibodies against VAP-A and Myc. High magnifications of the boxed areas are shown in the insets. Scale bars: 10  $\mu\text{m}$  (large panels); 5  $\mu\text{m}$  (insets).

cells, VAP-A and VAP-B strongly accumulated in the juxtannuclear compartments (Figure 9A). Although expression of PH-FFAT did not enhance juxtannuclear accumulation of GFP-Sac1 other than slightly increasing the peripheral signals, live-cell imaging showed that the mobility of the GFP-Sac1-positive compartments was significantly reduced upon expression of PH-FFAT-monomeric red fluorescent protein (mRFP), compared with the control (Supplemental Movie S1). These results support the idea that ER-Golgi contacts were immobilized by expression of PH-FFAT. Next we tested the effects of expression of PH-FFAT on PAUF secretion and CARTS biogenesis. Our data indicate that Myc-PH-FFAT expression completely blocked the secretion of PAUF-MycHis (Figure 9B). We also found that the average number of PAUF-MycHis-containing CARTS was significantly decreased in cells expressing PH-FFAT-mRFP (Figure 9, C and D). These results suggest that the association-dissociation dynamics of ER and Golgi membranes are important for producing CARTS at the TGN.

## DISCUSSION

Our work revealed that VAP-A/B knockdown impaired the processing and secretion of PAUF, which is one of the cargo proteins of CARTS. Similar effects were caused by D-ceramide-C6 treatment or disruption of the functions of CERT and OSBP, suggesting the requirement of VAP-mediated nonvesicular lipid transfer between the ER and the Golgi complex for PAUF processing and secretion. An *in vivo* analysis and an analysis with biochemical CARTS formation assay showed that VAPs are required for CARTS biogenesis at the TGN. A series of our experiments suggest that VAPs form complexes with CERT and OSBP/Sac1, respectively, at specialized ER subdomains where the *trans*-Golgi/TGN membranes are closely apposed and two organelles are thought to form membrane contact sites. Our results also suggest that the association-dissociation dynamics of ER-Golgi contacts are important for PAUF secretion and CARTS biogenesis. On the basis of these findings, we

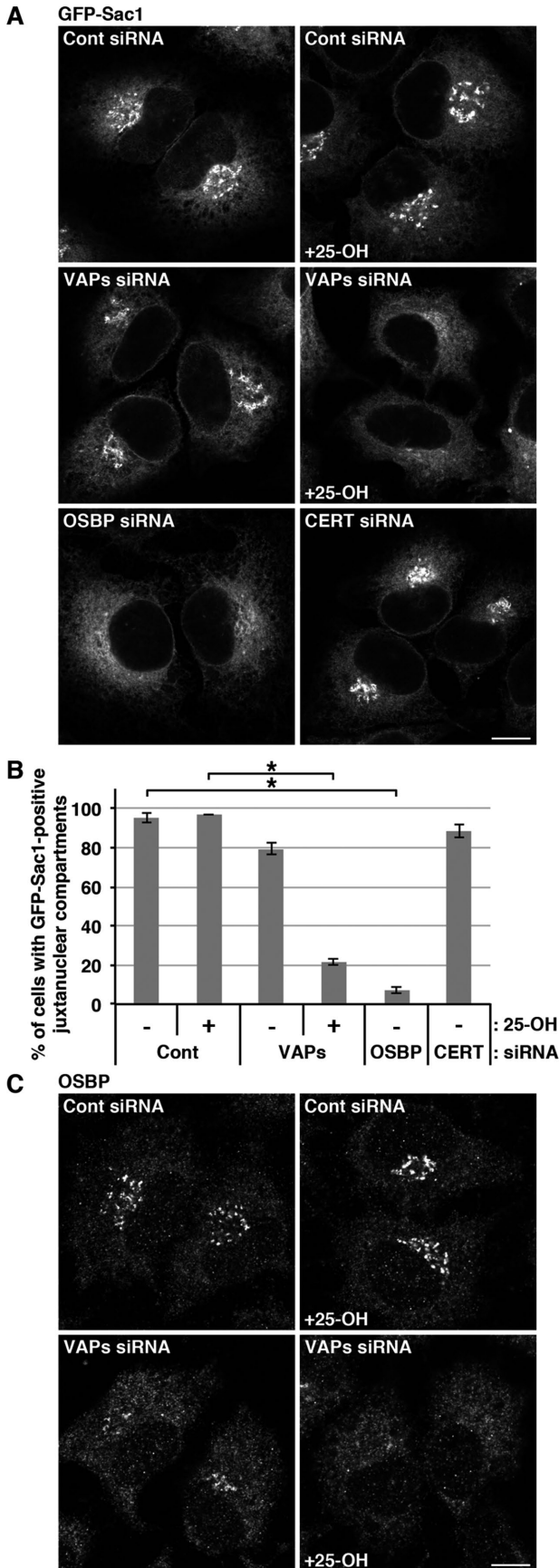


**FIGURE 7:** Knockdown of VAP-A/B and OSBP inhibits juxtannuclear accumulations of Sac1. (A–C) HeLa cells stably expressing GFP-Sac1 were transfected with control (Cont) siRNA, a mixture of siRNA oligos

propose the model shown in Figure 10. At ER–Golgi contact sites VAP-CERT and VAP-OSBP-Sac1 complexes transport ceramide and cholesterol, respectively, from the ER to the *trans*-Golgi/TGN. Ceramide and PC are then metabolized to SM and DAG by SM synthase. Both these lipids play an essential role in the biogenesis of CARTS. DAG recruits PKD to the TGN membrane, and PKD causes membrane scission by activating downstream targets (Malhotra and Campelo, 2011). In addition, SM and cholesterol facilitate the formation of membrane microdomains, which function as a platform of molecular machineries responsible for cargo processing and sorting and membrane bending (Simons and van Meer, 1988; Gkantiragas *et al.*, 2001; Klemm *et al.*, 2009; Surma *et al.*, 2011; Duran *et al.*, 2012; van Galen *et al.*, 2014). Impaired processing of PAUF in VAP-A/B knockdown cells could be due to a glycosylation defect as a consequence of disruption of functional enzymatic domains at the TGN, as previously observed upon D-ceramide-C6 treatment (van Galen *et al.*, 2014).

Formation of ER–Golgi contacts is under control of proteins and lipids. Our data suggest that recruitment of Sac1 to juxtannuclear ER subdomains requires OSBP, the recruitment of which to the ER–Golgi contact sites, in turn, needs VAPs (Figure 10, middle, right). Because overexpression of Sac1 inhibited OSBP recruitment, there might be mutual regulation. Phosphoinositides are thought to play an important role in these processes. Both OSBP and CERT interact with PI4P through their PH domain for targeting to the PI4P-rich Golgi compartment (Levine and Munro, 2002; Hanada *et al.*, 2003). Therefore VAP/OSBP-mediated reciprocal transfer of PI4P to the ER could regulate the association of OSBP and CERT with the *trans*-Golgi/TGN membrane. At the ER, Sac1 hydrolyzes PI4P to PI for maintaining the PI4P gradient between the ER and the *trans*-Golgi/TGN, which ensures the direction of nonvesicular lipid transfer. PI is likely to be transported back to the *trans*-Golgi/TGN by the VAP-Nir2 complex at ER–Golgi contact sites (Kim *et al.*, 2013; Peretti *et al.*, 2008). At the Golgi complex, PI is phosphorylated by phosphatidylinositol 4-kinases (PI4Ks) to produce PI4P (Weixel *et al.*, 2005; Tóth *et al.*, 2006; Banerji *et al.*, 2010; Graham and Burd, 2011; Bankaitis *et al.*, 2012; Kim *et al.*, 2013). Because PKD phosphorylates and activates PI4KIII $\beta$  (Hausser *et al.*, 2005), there seems to be an activation loop within the lipid transfer mechanism. Therefore this system might be used for local concentration of the lipids responsible for transport carrier biogenesis. PKD also phosphorylates CERT and OSBP to release these proteins from the Golgi membrane (Fugmann *et al.*, 2007; Nhek *et al.*, 2010; Olayioye and Hausser, 2012), which could facilitate continuous rounds of lipid transfer at the restricted sites. In this context, ER–Golgi contacts might define the sites of membrane scission, and this is reminiscent of the findings of the roles of ER contact sites in mitochondria and endosome fission (Friedman *et al.*, 2011; Rowland *et al.*, 2014). It is worth noting that the small GTPase ADP-ribosylation

for VAP-A (523) and VAP-B (498), OSBP siRNA, or CERT siRNA. After 20 h, the cells were washed and incubated with fresh medium. At 72 h after siRNA transfection, the cells were treated with or without 2  $\mu$ g/ml 25-OH for 2.5 h, fixed, and visualized with GFP (A) and an anti-OSBP antibody (C). Scale bars: 10  $\mu$ m. (B) Quantification of Sac1 accumulations at juxtannuclear ER subdomains. The percentage of control, VAP-A/B, OSBP, and CERT knockdown cells with GFP-Sac1-positive juxtannuclear compartments ( $n = 202$ – $250$  cells per condition) in the presence or absence of 25-OH was determined, and the average values of three independent experiments are shown (mean  $\pm$  SD). Asterisks indicate  $p < 0.0001$ .

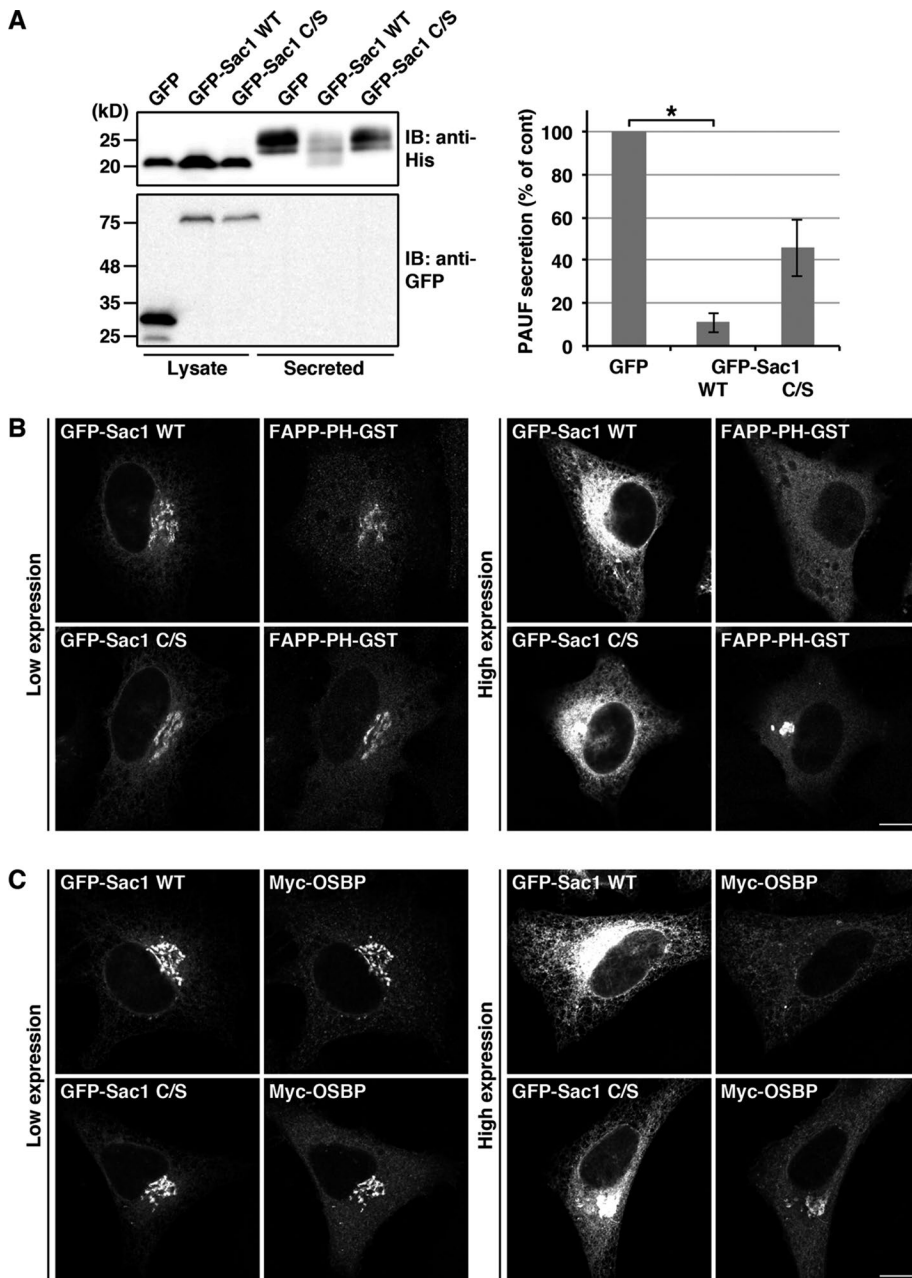


**FIGURE 8:** Overexpression of Sac1 inhibits PAUF processing and secretion in a phosphatase activity-dependent manner. (A) HEK 293T cells were cotransfected with plasmids for PAUF-MycHis and GFP (control) or GFP-Sac1 wild type (WT) or C/S. After 20 h, the cells were washed and incubated with fresh medium for 4 h. The medium and the cell lysate were Western blotted with the indicated antibodies. The amount of secreted PAUF was normalized with the total cellular levels. The average values of four independent experiments are shown (mean  $\pm$  SD). Asterisk indicates  $p < 0.02$ . (B and C) HeLa cells were cotransfected with a plasmid for FAPP-PH-GST (B) or Myc-OSBP (C) in combination with a plasmid for GFP-Sac1 wild type or C/S, fixed, and visualized with GFP and an antibody against GST or Myc. Scale bars: 10  $\mu$ m.

factor 1 (Arf1) is also important for the binding of OSBP, PI4KIII $\beta$ , and PKD to the Golgi membrane (Godi *et al.*, 1999; Levine and Munro, 2002; Pusapati *et al.*, 2010). Considering the roles of Arf1 in vesicular coat formation at the Golgi complex (D'Souza-Schorey and Chavrier, 2006), Arf1 likely not only acts as a scaffold but also coordinates transport carrier biogenesis with the lipid transfer at ER-Golgi contact sites.

A protein complex of VAPs, OSBP, and Sac1 is similar to previously reported protein interactions in yeast between Scs2/Scs22 (VAP orthologues), Osh3 (OSBP orthologue), and Sac1 at ER-PM contact sites (Stefan *et al.*, 2011; 2013). In yeast, Ist2 (related to mammalian TMEM16 ion channels), tricalbins (orthologues of the extended synaptotagmins), and Scs2/Scs22 tether the ER membrane to the PM (Manford *et al.*, 2012). The involvement of the extended synaptotagmins in the formation of ER-PM contacts has been also shown in mammalian cells (Giordano *et al.*, 2013). In addition, the ER-localized SNARE Sec22b was found to form a nonfusogenic *trans*-SNARE complex with PM-localized syntaxin 1 at ER-PM contact sites (Petkovic *et al.*, 2014). Compared with these findings, the molecular machineries for ER-Golgi tethering are poorly understood. Because of the high density of the ER membrane in the perinuclear region, scrutiny of ER-Golgi contacts by fluorescence microscopy is relatively difficult. In this study, we found that Sac1 shows a significant accumulation at juxtannuclear ER subdomains closely apposed to the *trans*-Golgi/TGN in a steady state, suggesting that this protein will be a useful marker to monitor ER-Golgi contacts.

In conclusion, our study demonstrates the requirement of VAPs for CARTS biogenesis and provides evidence that complexes of VAPs and lipid transfer proteins function at ER-Golgi contact sites, which highlights the significance of ER-Golgi contacts in lipid signaling leading to transport carrier formation from the TGN.

## MATERIALS AND METHODS

### Antibodies and reagents

Monoclonal antibodies against His, Myc, FLAG, HA, calnexin, and SERCA2 were purchased from Qiagen (Hilden, Germany), Santa Cruz Biotechnology (Santa Cruz, CA), Sigma-Aldrich (St. Louis, MO), Roche (Mannheim, Germany), BD Biosciences (San Jose, CA), and Millipore (Billerica, MA), respectively. Polyclonal antibodies were procured as follows: TGN46 was purchased from AbD Serotec (Oxford, UK); GST and HA from Santa Cruz Biotechnology; Myc from Cell Signaling Technology (Beverly, MA); OSBP from Proteintech (Chicago, IL); and GFP from Molecular Probes (Eugene, OR). To raise polyclonal antibodies against VAP-A and VAP-B, GST-tagged fragments of human VAP-A (aa 8–215) and VAP-B (aa 1–223), respectively, were expressed in *Escherichia coli*, purified, and used as antigens. The rabbit polyclonal antibodies against VAP-A and VAP-B were isolated by affinity chromatography on antigen-coupled beads. Anti-VIMP polyclonal antibody was produced

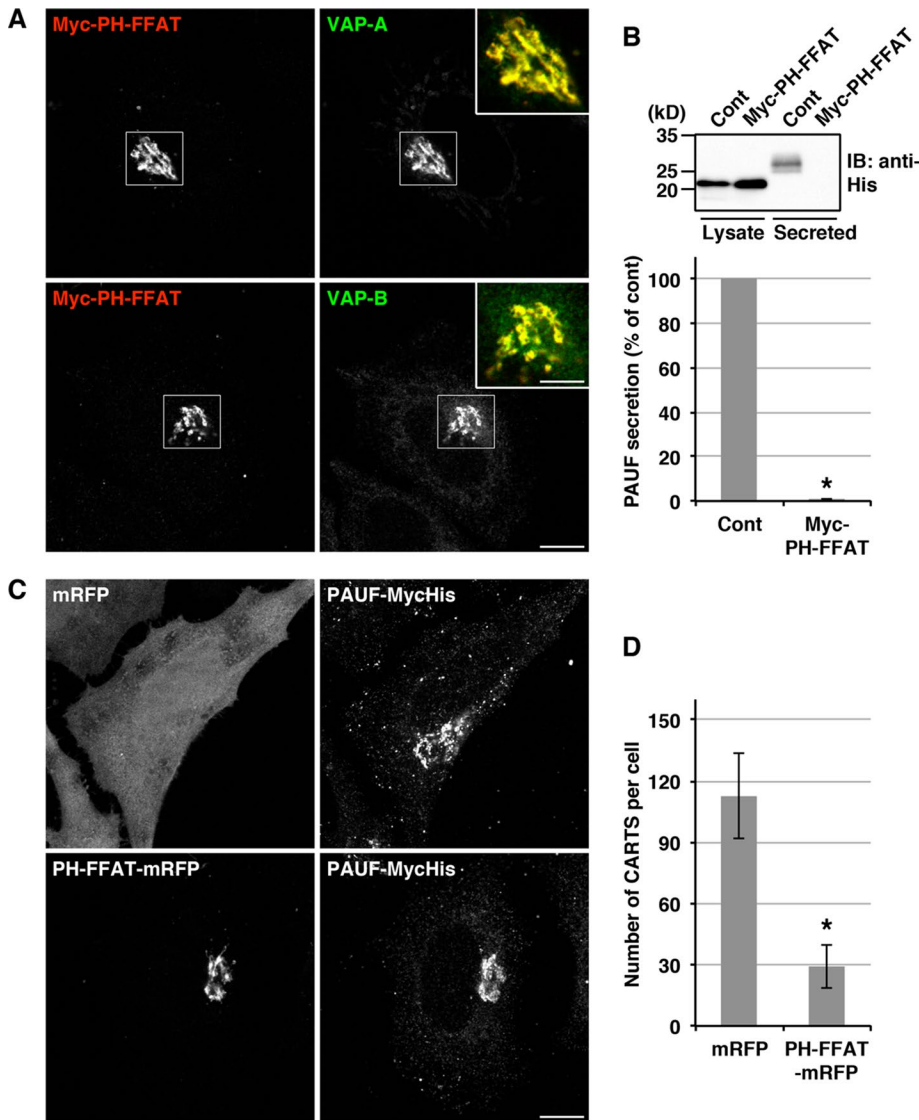


**FIGURE 9:** Immobilization of ER–Golgi contacts impairs PAUF secretion and CARTS biogenesis. (A) HeLa cells were transfected with a plasmid for Myc-PH-FFAT, fixed, and visualized with antibodies against Myc and VAP-A or VAP-B. High magnifications of merged images of the boxed areas are shown in the insets. Scale bars: 10  $\mu$ m (large panels); 5  $\mu$ m (insets). (B) HEK 293T cells were transfected with a PAUF-MycHis plasmid alone (control) or with a PAUF-MycHis plasmid in combination with a plasmid for Myc-PH-FFAT. After 20 h, the cells were washed and incubated with fresh medium for 4 h. Western blotting and quantification were performed as in Figure 1D. Asterisk indicates  $p < 0.04$ . (C) HeLa cells stably expressing PAUF-MycHis were transfected with a plasmid for mRFP (control) or PH-FFAT-mRFP, fixed, and visualized with mRFP and an anti-Myc antibody. Scale bar: 10  $\mu$ m. (D) Quantification of PAUF-MycHis-containing CARTS. The number of CARTS in mRFP-expressing cells ( $n = 1128$  punctate elements in 10 cells) and PH-FFAT-mRFP-expressing cells ( $n = 289$  punctate elements in 10 cells) was determined (mean  $\pm$  SD). Asterisk indicates  $p < 0.0001$ .

as described previously (Noda *et al.*, 2014). Nocodazole, D-ceramide-C6 (*N*-hexanoyl-D-sphingosin), and 25-OH were purchased from Sigma-Aldrich.

#### Plasmids

The plasmids encoding PAUF-MycHis, GFP-GT, Myc-OSBP, HA-CERT, and FAPP-PH-GST were kindly donated by S. S. Koh (Korea Research Institute of Bioscience and Biotechnology, Daejeon, Korea), J. Lippincott-Schwartz (National Institutes of

Health, Bethesda, MD), H. Arai (University of Tokyo, Tokyo, Japan), K. Hanada (National Institute of Infectious Diseases, Tokyo, Japan), and M. A. De Matteis (Telethon Institute of Genetics and Medicine, Pozzuoli [Naples], Italy), respectively. The plasmids encoding GFP-Sac1 wild type and C/S mutant were generous gifts from P. Mayinger (Oregon Health and Science University, Portland, OR). The plasmids encoding GST-C1a-PKD1 and GST-PKD2 wild type were provided by V. Malhotra (Centre for Genomic Regulation, Barcelona, Spain). A point mutation (FF/AA) in CERT and OSBP was introduced into plasmids for HA-CERT and Myc-OSBP, respectively, by PCR using primers designed for replacing two phenylalanines in the FFAT motif with alanines in the expressed proteins. The cDNA encoding PH-FFAT (aa 78–410 of rabbit OSBP) was inserted into pCMV-Tag 3A and a pcDNA3-based plasmid encoding mRFP to express the protein with an N-terminal Myc and a C-terminal mRFP, respectively. The cDNA encoding human Sac1 was inserted into pFLAG-CMV-6c to express the protein with an N-terminal FLAG. The cDNA encoding GFP-Sac1 or PAUF-MycHis was inserted into pCI-IRES-Bsr (Yonekawa *et al.*, 2011) to establish stable cell lines.

#### Cell culture and transfection

HeLa and HEK 293T cells were grown in DMEM supplemented with 10% fetal calf serum. HeLa cells stably expressing GFP-Sac1 or PAUF-MycHis were selected with 10  $\mu$ g/ml blasticidin S. Plasmid and siRNA transfection into HeLa cells was carried out using X-tremeGENE 9 DNA transfection reagent (Roche) and Oligofectamine reagent (Invitrogen, Carlsbad, CA), respectively, according to the manufacturers' protocols. Plasmid transfection into HEK 293T cells was carried out using Lipofectamine 2000 transfection reagent (Invitrogen), according to the manufacturer's protocol.

#### RNA interference

The sequences of siRNA oligos were as follows:

Control (GL2 luciferase): 5'-CGUACGCGGAAUACUUCGA-3'

VAP-A (148): 5'-AGUGAAGACUACAGCACCU-3'

VAP-A (523): 5'-CUAUGGAAGAGUGUAAAA-3'

VAP-B (353): 5'-CUUAGAUGUGUUUGAAU-3'

VAP-B (498): 5'-GAAGGUUAUGGAAGAAUGU-3'

CERT: 5'-GAACAGAGGAAGCAUUA-3'

OSBP: 5'-UACUGGGAGUGUAAAGAAA-3'

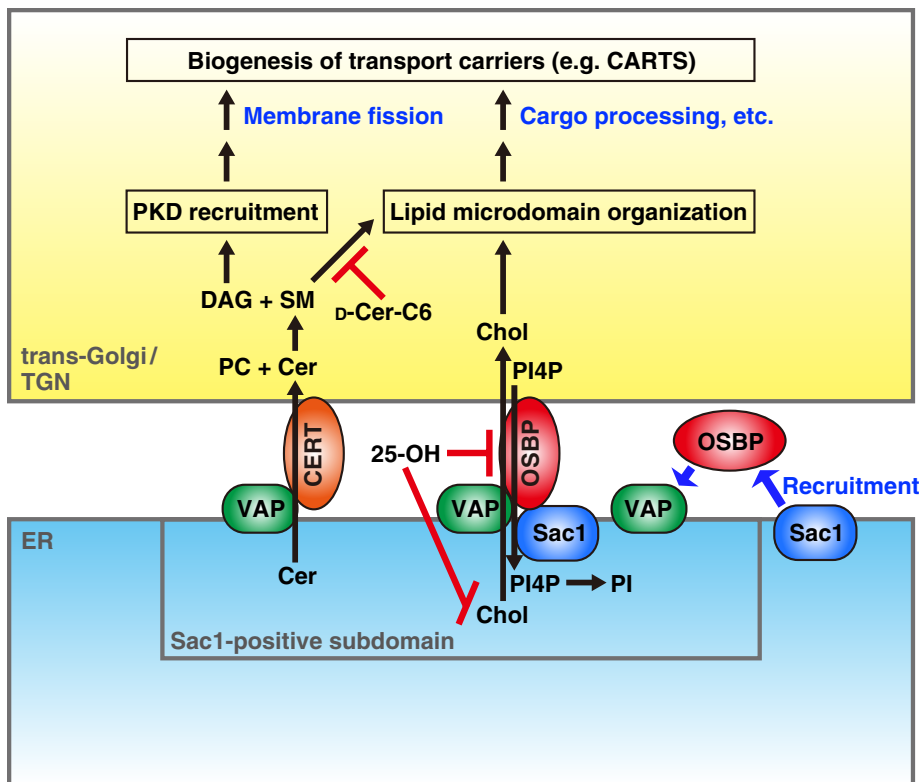


**FIGURE 10:** Working model for ER–Golgi contact-mediated regulation of transport carrier biogenesis. Ceramide (Cer) and cholesterol (Chol) are transported from the ER to the *trans*-Golgi/TGN by VAP-CERT and VAP-OSBP-Sac1 complexes, respectively, at the membrane contact site. CARTS biogenesis is controlled in two ways: 1) DAG-dependent recruitment of PKD and 2) cholesterol- and SM-rich microdomain organization. PI4P transported from the *trans*-Golgi/TGN to the ER is hydrolyzed by Sac1, which is recruited to a VAP-OSBP complex formed at a specialized ER subdomain closely apposed to the *trans*-Golgi/TGN. Reagents used in this study are also shown: 25-OH treatment inhibits both cholesterol synthesis and transfer; D-ceramide-C6 (D-Cer-C6) treatment disrupts cholesterol- and SM-rich microdomain organization.

### PAUF secretion assay

HeLa cells were transfected with control siRNA or siRNA oligos targeting VAP-A and VAP-B. At 48 h after siRNA transfection, cells were transfected with a plasmid for PAUF-MyHis; 20 h later, the medium was replaced with Opti-MEM and incubated at 37°C for the indicated time points. After the medium was collected, cells were lysed with 0.5% SDS and 0.025 U/μl Benzonase nuclease (Sigma-Aldrich) in phosphate-buffered saline (PBS). The medium and cell lysates were analyzed by Western blotting with an anti-His antibody. For experiments with D-ceramide-C6, PAUF-MyHis-expressing cells were pretreated with ethanol (control) or 5 μM D-ceramide-C6 for 2.5 h and then incubated with fresh Opti-MEM containing each reagent for 3 h. Secreted proteins in the medium were precipitated with trichloroacetic acid, and the precipitates and cell lysates were Western blotted with an anti-His antibody.

### RT-PCR

RNA was prepared using the RNeasy Mini kit (Qiagen), and cDNA was synthesized with the SuperScript III reverse transcriptase (Invitrogen) primed by oligo(dT)15. Each cDNA was amplified by PCR with the following primers:

CERT (457 base pairs): 5'-AGTATGGCTGCAGAGGATCC-3' and 5'-CCATCAGAACGCGTTGTAGG-3'

OSBP (410 base pairs): 5'-AAAGCTGTGAAGATGCTGGC-3' and 5'-AGGTGATTATGCTGCTTCGC-3'

β-actin (234 base pairs): 5'-GGACTTCGAGCAAGAGATGG-3' and 5'-AGCATCTGTGTTGGCGTACAG-3'

### Immunofluorescence microscopy

Cells were fixed with 4% paraformaldehyde in PBS at room temperature for 20 min, permeabilized with 0.2% Triton X-100 in PBS for 30 min, and then blocked with 2% bovine serum albumin (BSA) in PBS for 30 min. For endogenous OSBP staining, cells were fixed with methanol at –20°C for 5 min and blocked with 2% BSA in PBS for 30 min. The cells were labeled with the indicated primary antibodies and secondary antibodies conjugated to Alexa Fluor 488, 546, 594, or 633. The samples were analyzed with an Olympus Fluoview FV1000 confocal microscope with a UPLSAPO 60×/1.35 NA objective and FV10-ASW software. Image processing, quantification of CARTS, and measurement of fluorescence intensity were performed with ImageJ software (National Institutes of Health). The fluorescence signal of PAUF-MyHis-containing punctae was distinguished from the background by setting a threshold and was analyzed at a set size within 0.05–2.00 μm<sup>2</sup>.

### CARTS formation assay

CARTS formation assay was performed as described previously (Wakana et al., 2012).

In brief, 72 h after siRNA transfection, HeLa cells were treated with 2 μg/ml 25-OH for 2.5 h, and the cells were suspended in buffer A (20 mM HEPES-KOH, pH 7.4, 250 mM D-sorbitol, and 150 mM potassium acetate), permeabilized with 40 μg/ml digitonin, and then washed with buffer A supplemented with 1 M KCl. The permeabilized cells (3.4 × 10<sup>5</sup> cells/ml) were incubated at 32°C for 45 min in buffer A supplemented with an ATP-regenerating system (1 mM ATP, 40 mM creatine phosphate, and 0.2 mg/ml creatine kinase) and 0.5 mg/ml rat liver cytosol. Transport carriers were separated by two sequential steps of centrifugation at 10,000 × g (low speed) and at 100,000 × g (high speed). The pellet was Western blotted with an anti-TGN46 antibody to estimate the amount of CARTS generated.

### Live-cell imaging

HeLa cells stably expressing GFP-Sac1 were transfected with a plasmid for mRFP or PH-FFAT-mRFP. After 20 h, the medium was replaced with Opti-MEM, and cells were maintained in 5% CO<sub>2</sub> at 37°C during live-cell imaging. Images were acquired continuously with time intervals between frames of 5 s for ~10 min by use of an Olympus Fluoview FV1000 confocal microscope with a UPLSAPO 60×/1.35 NA objective and FV10-ASW software. The images were processed with ImageJ software.

### Fluorescence loss in photobleaching

HeLa cells stably expressing GFP-Sac1 or GFP-GT in Opti-MEM were cultured in 5% CO<sub>2</sub> at 37°C during live-cell imaging. The cells

were subjected to bleaching with high laser intensity (473-nm laser) for 15 s followed by an imaging scan with time intervals between frames of 10 s for ~6 min by use of an Olympus Fluoview FV1000 confocal microscope with a UPLSAPO 100×/1.40 NA objective and FV10-ASW software. Image processing and measurement of fluorescence intensity were performed with ImageJ software.

### Immunoprecipitation

HEK 293T cells were lysed in buffer B (50 mM HEPES-KOH, pH 7.4, 100 mM NaCl, 1.5 mM MgCl<sub>2</sub>, 1 mM dithiothreitol, 1% Nonidet P-40, 1 μg/ml leupeptin, 2 μM pepstatin A, 2 μg/ml aprotinin, and 1 mM phenylmethylsulfonyl fluoride). The lysates were centrifuged at 17,000 × *g* for 10 min. The resulting supernatants were immunoprecipitated with anti-FLAG beads (Sigma-Aldrich), and the precipitated proteins were analyzed by Western blotting.

### PLA

PLA was performed using the Duolink kit (Sigma-Aldrich) according to the manufacturer's protocol.

### ACKNOWLEDGMENTS

We thank Peter Mayinger, Hiroyuki Arai, Kentaro Hanada, Jennifer Lippincott-Schwartz, Sang Seok Koh, Maria Antonietta De Matteis, and Vivek Malhotra for providing materials. We appreciate the technical assistance of Rei Okuma, Yoshinobu Izumi, and Akiko Furuno. We are grateful to Josse van Galen, Christopher G. Burd, Suzanne R. Pfeffer, and Vivek Malhotra for comments on the manuscript. This work was supported in part by Grants-in-Aid for Scientific Research (grants 25291029 to M.T. and 25840042 to Y.W.) from the Ministry of Education, Culture, Sports, Science, and Technology of Japan; the NOVARTIS Foundation (Japan) for the Promotion of Science (to Y.W.); and the Uehara Memorial Foundation (to Y.W.).

### REFERENCES

- Alpy F, Rousseau A, Schwab Y, Legueux F, Stoll I, Wendling C, Spiegelhalter C, Kessler P, Mathelin C, Rio MC, et al. (2013). STARD3 or STARD3NL and VAP form a novel molecular tether between late endosomes and the ER. *J Cell Sci* 126, 5500–5512.
- Balch WE, Glick BS, Rothman JE (1984). Sequential intermediates in the pathway of intercompartmental transport in a cell-free system. *Cell* 39, 525–536.
- Banerji S, Ngo M, Lane CF, Robinson CA, Minogue S, Ridgway ND (2010). Oxysterol binding protein-dependent activation of sphingomyelin synthesis in the Golgi apparatus requires phosphatidylinositol 4-kinase IIα. *Mol Biol Cell* 21, 4141–4150.
- Bankaitis VA, Garcia-Mata R, Mousley CJ (2012). Golgi membrane dynamics and lipid metabolism. *Curr Biol* 22, R414–R424.
- Baron CL, Malhotra V (2002). Role of diacylglycerol in PKD recruitment to the TGN and protein transport to the plasma membrane. *Science* 295, 325–328.
- Blagoveshchenskaya A, Cheong FY, Rohde HM, Glover G, Knödler A, Nicolson T, Boehmelt G, Mayinger P (2008). Integration of Golgi trafficking and growth factor signaling by the lipid phosphatase SAC1. *J Cell Biol* 180, 803–812.
- Brown MS, Goldstein JL (1974). Suppression of 3-hydroxy-3-methylglutaryl coenzyme A reductase activity and inhibition of growth of human fibroblasts by 7-ketocholesterol. *J Biol Chem* 249, 7306–7314.
- Cole NB, Sciaky N, Marotta A, Song J, Lippincott-Schwartz J (1996). Golgi dispersal during microtubule disruption: regeneration of Golgi stacks at peripheral endoplasmic reticulum exit sites. *Mol Biol Cell* 7, 631–650.
- Dippold HC, Ng MM, Farber-Katz SE, Lee SK, Kerr ML, Peterman MC, Sim R, Wiharto PA, Galbraith KA, Madhavarapu S, et al. (2009). GOLPH3 bridges phosphatidylinositol-4-phosphate and actomyosin to stretch and shape the Golgi to promote budding. *Cell* 139, 337–351.
- Dowler S, Currie RA, Campbell DG, Deak M, Kular G, Downes CP, Alessi DR (2000). Identification of pleckstrin-homology-domain-containing proteins with novel phosphoinositide-binding specificities. *Biochem J* 351, 19–31.
- D'Souza-Schorey C, Chavrier P (2006). ARF proteins: roles in membrane traffic and beyond. *Nat Rev Mol Cell Biol* 7, 347–358.
- Duran JM, Campelo F, van Galen J, Sachsenheimer T, Sot J, Egorov MV, Rentero C, Enrich C, Polishchuk RS, Goñi FM, et al. (2012). Sphingomyelin organization is required for vesicle biogenesis at the Golgi complex. *EMBO J* 31, 4535–4546.
- Friedman JR, Lackner LL, West M, DiBenedetto JR, Nunnari J, Voeltz GK (2011). ER tubules mark sites of mitochondrial division. *Science* 334, 358–362.
- Fugmann T, Hausser A, Schöffler P, Schmid S, Pfizenmaier K, Olayioye MA (2007). Regulation of secretory transport by protein kinase D-mediated phosphorylation of the ceramide transfer protein. *J Cell Biol* 178, 15–22.
- Giordano F, Saheki Y, Idevall-Hagren O, Colombo SF, Pirruccello M, Milosevic I, Gracheva EO, Bagriantsev SN, Borgese N, De Camilli P (2013). PI(4,5)P(2)-dependent and Ca(2+)-regulated ER-PM interactions mediated by the extended synaptotagmins. *Cell* 153, 1494–1509.
- Gkantrigas I, Brügger B, Stüven E, Kaloyanova D, Li XY, Löhr K, Lottspeich F, Wieland FT, Helms JB (2001). Sphingomyelin-enriched microdomains at the Golgi complex. *Mol Biol Cell* 12, 1819–1833.
- Godi A, Pertile P, Meyers R, Marra P, Di Tullio G, Iurisci C, Luini A, Corda D, De Matteis MA (1999). ARF mediates recruitment of PtdIns-4-OH kinase-beta and stimulates synthesis of PtdIns(4,5)P2 on the Golgi complex. *Nat Cell Biol* 1, 280–287.
- Graham TR, Burd CG (2011). Coordination of Golgi functions by phosphatidylinositol 4-kinases. *Trends Cell Biol* 21, 113–121.
- Hammond GR, Machner MP, Balla T (2014). A novel probe for phosphatidylinositol 4-phosphate reveals multiple pools beyond the Golgi. *J Cell Biol* 205, 113–126.
- Hanada K, Kumagai K, Tomishige N, Yamaji T (2009). CERT-mediated trafficking of ceramide. *Biochim Biophys Acta* 1791, 684–691.
- Hanada K, Kumagai K, Yasuda S, Miura Y, Kawano M, Fukasawa M, Nishijima M (2003). Molecular machinery for non-vesicular trafficking of ceramide. *Nature* 426, 803–809.
- Hausser A, Storz P, Märtens S, Link G, Toker A, Pfizenmaier K (2005). Protein kinase D regulates vesicular transport by phosphorylating and activating phosphatidylinositol-4 kinase IIIβ at the Golgi complex. *Nat Cell Biol* 7, 880–886.
- Huitema K, van den Dikkenberg J, Brouwers JF, Holthuis JC (2004). Identification of a family of animal sphingomyelin synthases. *EMBO J* 23, 33–44.
- Kandutsch AA, Chen HW (1974). Inhibition of sterol synthesis in cultured mouse cells by cholesterol derivatives oxygenated in the side chain. *J Biol Chem* 249, 6057–6061.
- Kawano M, Kumagai K, Nishijima M, Hanada K (2006). Efficient trafficking of ceramide from the endoplasmic reticulum to the Golgi apparatus requires a VAMP-associated protein-interacting FFAT motif of CERT. *J Biol Chem* 281, 30279–30288.
- Kim SA, Lee Y, Jung DE, Park KH, Park JY, Gang J, Jeon SB, Park EC, Kim YG, Lee B, et al. (2009). Pancreatic adenocarcinoma up-regulated factor (PAUF), a novel up-regulated secretory protein in pancreatic ductal adenocarcinoma. *Cancer Sci* 100, 828–836.
- Kim YJ, Hernandez ML, Balla T (2013). Inositol lipid regulation of lipid transfer in specialized membrane domains. *Trends Cell Biol* 23, 270–278.
- Klemm RW, Ejsing CS, Surma MA, Kaiser HJ, Gerl MJ, Sampaio JL, de Robillard Q, Ferguson C, Proszynski TJ, Shevchenko A, et al. (2009). Segregation of sphingolipids and sterols during formation of secretory vesicles at the trans-Golgi network. *J Cell Biol* 185, 601–612.
- Ladinsky MS, Mastrorade DN, McIntosh JR, Howell KE, Staehelin LA (1999). Golgi structure in three dimensions: functional insights from the normal rat kidney cell. *J Cell Biol* 144, 1135–1149.
- Lev S, Ben Halevy D, Peretti D, Dahan N (2008). The VAP protein family: from cellular functions to motor neuron disease. *Trends Cell Biol* 18, 282–290.
- Levine TP, Munro S (2002). Targeting of Golgi-specific pleckstrin homology domains involves both PtdIns 4-kinase-dependent and -independent components. *Curr Biol* 12, 695–704.
- Liljedahl M, Maeda Y, Colanzi A, Ayala I, Van Lint J, Malhotra V (2001). Protein kinase D regulates the fission of cell surface destined transport carriers from the trans-Golgi network. *Cell* 104, 409–420.
- Lingwood D, Simons K (2010). Lipid rafts as a membrane-organizing principle. *Science* 327, 46–50.
- Liu Y, Boukhelifa M, Tribble E, Morin-Kensicki E, Uetrecht A, Bear JE, Bankaitis VA (2008). The Sac1 phosphoinositide phosphatase regulates

- Golgi membrane morphology and mitotic spindle organization in mammals. *Mol Biol Cell* 19, 3080–3096.
- Loewen CJ, Roy A, Levine TP (2003). A conserved ER targeting motif in three families of lipid binding proteins and in Opi1p binds VAP. *EMBO J* 22, 2025–2035.
- Loewen CJ, Young BP, Tavassoli S, Levine TP (2007). Inheritance of cortical ER in yeast is required for normal septin organization. *J Cell Biol* 179, 467–483.
- Maeda Y, Beznoussenko GV, Van Lint J, Mironov AA, Malhotra V (2001). Recruitment of protein kinase D to the *trans*-Golgi network via the first cysteine-rich domain. *EMBO J* 20, 5982–5990.
- Malhotra V, Campelo F (2011). PKD regulates membrane fission to generate TGN to cell surface transport carriers. *Cold Spring Harb Perspect Biol* 3, a005280.
- Malhotra V, Serafini T, Orci L, Shepherd JC, Rothman JE (1989). Purification of a novel class of coated vesicles mediating biosynthetic protein transport through the Golgi stack. *Cell* 58, 329–336.
- Manford AG, Stefan CJ, Yuan HL, Macgurn JA, Emr SD (2012). ER-to-plasma membrane tethering proteins regulate cell signaling and ER morphology. *Dev Cell* 23, 1129–1140.
- Mesmin B, Bigay J, Moser von Filseck J, Lacas-Gervais S, Drin G, Antony B (2013). A four-step cycle driven by PI(4)P hydrolysis directs sterol/PI(4)P exchange by the ER-Golgi tether OSBP. *Cell* 155, 830–843.
- Mogelvang S, Marsh BJ, Ladinsky MS, Howell KE (2004). Predicting function from structure: 3D structure studies of the mammalian Golgi complex. *Traffic* 5, 338–345.
- Ngo M, Ridgway ND (2009). Oxysterol binding protein-related protein 9 (ORP9) is a cholesterol transfer protein that regulates Golgi structure and function. *Mol Biol Cell* 20, 1388–1399.
- Nhek S, Ngo M, Yang X, Ng MM, Field SJ, Asara JM, Ridgway ND, Tokar A (2010). Regulation of oxysterol-binding protein Golgi localization through protein kinase D-mediated phosphorylation. *Mol Biol Cell* 21, 2327–2337.
- Nishimura Y, Hayashi M, Inada H, Tanaka T (1999). Molecular cloning and characterization of mammalian homologues of vesicle-associated membrane protein-associated (VAMP-associated) proteins. *Biochem Biophys Res Commun* 254, 21–26.
- Noda C, Kimura H, Arasaki K, Matsushita M, Yamamoto A, Wakana Y, Inoue H, Tagaya M (2014). Valosin-containing protein-interacting membrane protein (VIMP) links the endoplasmic reticulum with microtubules in concert with cytoskeleton-linking membrane protein (CLIMP)-63. *J Biol Chem* 289, 24304–24313.
- Olayioye MA, Hausser A (2012). Integration of non-vesicular and vesicular transport processes at the Golgi complex by the PKD-CERT network. *Biochim Biophys Acta* 1821, 1096–1103.
- Orci L, Glick BS, Rothman JE (1986). A new type of coated vesicular carrier that appears not to contain clathrin: its possible role in protein transport within the Golgi stack. *Cell* 46, 171–184.
- Peretti D, Dahan N, Shimoni E, Hirschberg K, Lev S (2008). Coordinated lipid transfer between the endoplasmic reticulum and the Golgi complex requires the VAP proteins and is essential for Golgi-mediated transport. *Mol Biol Cell* 19, 3871–3884.
- Perry RJ, Ridgway ND (2005). Molecular mechanisms and regulation of ceramide transport. *Biochim Biophys Acta* 1734, 220–234.
- Perry RJ, Ridgway ND (2006). Oxysterol-binding protein and vesicle-associated membrane protein-associated protein are required for sterol-dependent activation of the ceramide transport protein. *Mol Biol Cell* 17, 2604–2616.
- Petkovic M, Jemaiel A, Daste F, Specht CG, Izeddin I, Vorkel D, Verbavatz JM, Darzacq X, Triller A, Pfenninger KH, et al. (2014). The SNARE Sec22b has a non-fusogenic function in plasma membrane expansion. *Nat Cell Biol* 16, 434–444.
- Prescott AR, Lucocq JM, James J, Lister JM, Ponnambalam S (1997). Distinct compartmentalization of TGN46 and beta 1,4-galactosyltransferase in HeLa cells. *Eur J Cell Biol* 72, 238–246.
- Pusapati GV, Krndija D, Armacki M, von Wichert G, von Blume J, Malhotra V, Adler G, Seufferlein T (2010). Role of the second cysteine-rich domain and Pro275 in protein kinase D2 interaction with ADP-ribosylation factor 1, *trans*-Golgi network recruitment, and protein transport. *Mol Biol Cell* 21, 1011–1022.
- Rocha N, Kuijl C, van der Kant R, Janssen L, Houben D, Janssen H, Zwart W, Neeffjes J (2009). Cholesterol sensor ORP1L contacts the ER protein VAP to control Rab7-RILP-p150 Glued and late endosome positioning. *J Cell Biol* 185, 1209–1225.
- Rohde HM, Cheong FY, Konrad G, Paiha K, Mayinger P, Boehmelt G (2003). The human phosphatidylinositol phosphatase SAC1 interacts with the coatamer I complex. *J Biol Chem* 278, 52689–52699.
- Rowland AA, Chitwood PJ, Phillips MJ, Voeltz GK (2014). ER contact sites define the position and timing of endosome fission. *Cell* 159, 1027–1041.
- Shima DT, Haldar K, Pepperkok R, Watson R, Warren G (1997). Partitioning of the Golgi apparatus during mitosis in living HeLa cells. *J Cell Biol* 137, 1211–1228.
- Simons K, Ilkonen E (1997). Functional rafts in cell membranes. *Nature* 387, 569–572.
- Simons K, Sampaio JL (2011). Membrane organization and lipid rafts. *Cold Spring Harb Perspect Biol* 3, a004697.
- Simons K, van Meer G (1988). Lipid sorting in epithelial cells. *Biochemistry* 27, 6197–6202.
- Söderberg O, Gullberg M, Jarvius M, Ridderstråle K, Leuchowius KJ, Jarvius J, Wester K, Hydbring P, Bahram F, Larsson LG, et al. (2006). Direct observation of individual endogenous protein complexes in situ by proximity ligation. *Nat Methods* 3, 995–1000.
- Stefan CJ, Manford AG, Baird D, Yamada-Hanff J, Mao Y, Emr SD (2011). Osh proteins regulate phosphoinositide metabolism at ER-plasma membrane contact sites. *Cell* 144, 389–401.
- Stefan CJ, Manford AG, Emr SD (2013). ER-PM connections: sites of information transfer and inter-organelle communication. *Curr Opin Cell Biol* 25, 434–442.
- Surma MA, Klose C, Klemm RW, Ejsing CS, Simons K (2011). Generic sorting of raft lipids into secretory vesicles in yeast. *Traffic* 12, 1139–1147.
- Tóth B, Balla A, Ma H, Knight ZA, Shokat KM, Balla T (2006). Phosphatidylinositol 4-kinase III $\beta$  regulates the transport of ceramide between the endoplasmic reticulum and Golgi. *J Biol Chem* 281, 36369–36377.
- van Galen J, Campelo F, Martínez-Alonso E, Scarpa M, Martínez-Menárguez JÁ, Malhotra V (2014). Sphingomyelin homeostasis is required to form functional enzymatic domains at the *trans*-Golgi network. *J Cell Biol* 206, 609–618.
- Wakana Y, van Galen J, Meissner F, Scarpa M, Polishchuk RS, Mann M, Malhotra V (2012). A new class of carriers that transport selective cargo from the *trans* Golgi network to the cell surface. *EMBO J* 31, 3976–3990.
- Wakana Y, Villeneuve J, van Galen J, Cruz-Garcia D, Tagaya M, Malhotra V (2013). Kinesin-5/Eg5 is important for transport of CARTS from the *trans*-Golgi network to the cell surface. *J Cell Biol* 202, 241–250.
- Wang J, Chen J, Enns CA, Mayinger P (2013). The first transmembrane domain of lipid phosphatase SAC1 promotes Golgi localization. *PLoS One* 8, e71112.
- Weixel KM, Blumental-Perry A, Watkins SC, Aridor M, Weisz OA (2005). Distinct Golgi populations of phosphatidylinositol 4-phosphate regulated by phosphatidylinositol 4-kinases. *J Biol Chem* 280, 10501–10508.
- Wyles JP, McMaster CR, Ridgway ND (2002). Vesicle-associated membrane protein-associated protein-A (VAP-A) interacts with the oxysterol-binding protein to modify export from the endoplasmic reticulum. *J Biol Chem* 277, 29908–29918.
- Yonekawa S, Furuno A, Baba T, Fujiki Y, Ogasawara Y, Yamamoto A, Tagaya M, Tani K (2011). Sec16B is involved in the endoplasmic reticulum export of the peroxisomal membrane biogenesis factor peroxin 16 (Pex16) in mammalian cells. *Proc Natl Acad Sci USA* 108, 12746–12751.